Fluorescence and Coster-Kronig yields of the L_1 shell in gadolinium

T. Papp,[1,2] J. L. Campbell,[2] and S. Raman[3]
[1]*Institute of Nuclear Research of the Hungarian Academy of Sciences (ATOMKI), Debrecen H-4001, Postfach 51, Hungary*
[2]*Guelph-Waterloo Program for Graduate Work in Physics, University of Guelph, Guelph, Ontario, Canada N1G 2W1*
[3]*Physics Division, Oak Ridge National Laboratory, Oak Ridge, Tennessee 37831*
(Received 6 May 1998)

Using a Si(Li) x-ray spectrometer, we have measured the respective fractions of L_1, L_2, and L_3 x rays in the L x-ray spectrum emitted in the ^{157}Tb-^{157}Gd electron-capture decay. Using, in addition, our previously measured value for the ratio of L and K x rays, we deduce values for the fluorescence and Coster-Kronig yields of the L_1 subshell. These are $\omega_1 = 0.101 \pm 0.005$, $f_{12} = 0.166 \pm 0.020$, and $f_{13} = 0.287 \pm 0.014$. The f_{12} and f_{13} values are significantly below the predictions of the independent-particle model (IPM). The deduced L_1 level width of 3.7 eV is also significantly below the IPM width of 4.6 eV. [S1050-2947(98)01011-7]

PACS number(s): 32.70.Fw

I. INTRODUCTION

Vacancies in the atomic L_1 or L_2 level may deexcite via characteristic x-ray emission, Auger-electron emission, or the Coster-Kronig process. The latter involves a nonradiative transition in which the vacancy is filled by an electron from a higher L subshell with simultaneous ejection of a weakly bound outer-shell electron. An L_3 vacancy may deexcite only by the first two processes. The transition rates for the three processes have been calculated in the independent-particle model (IPM) by Scofield and by Chen *et al.*, who presented their results in a number of publications during the 1970s and 1980s. A full tabulation of these results, together with the relevant references, is given by Perkins *et al.* [1]. While both the Dirac-Fock (DF) and the Dirac-Hartree-Slater (DHS) potentials have been used to calculate radiative rates, the Perkins *et al.* compilation relies upon the DHS approach for both radiative and nonradiative rates.

Two quantities of great practical importance are derived from these rates. The first is the subshell fluorescence yield (ω_i, $i = 1,2,3$), i.e., the probability of L_i x-ray emission. The second is the Coster-Kronig probability (f_{ij}), i.e., the probability of nonradiative transfer of an L_i vacancy to the L_j subshell. The widely referenced paper of Chen, Crasemann, and Mark [2] presented IPM values of these six L subshell quantities based on DHS calculations. Accurate knowledge of the values of ω_i and f_{ij} as a function of atomic number Z is important in various contexts. One context is the extraction of inner-shell ionization cross sections by charged particles from measured x-ray spectra [3]. Another is the whole area of elemental analysis based upon x-ray emission spectroscopy techniques [4].

While theory is one source of values of ω_i and f_{ij}, an alternative and widely used source is a 1979 compendium [5] based upon the then available experimental data. Given the improvement in measurement technique since the date of that work, there is reason both to be cautious in adopting its recommendations, and to attempt improved measurements. Jitschin [6] has summarized more recent measurements, the accuracy of which is likely to be significantly better than those made before 1979. The situation for the L_2 and L_3 subshells appears moderately satisfactory. The measured fluorescence yields are in agreement with IPM theory at the 3% level. The measured Coster-Kronig probability f_{23} shows a well-defined trend to run 5–10 % below theory at the atomic numbers above $Z = 60$ where there are a large number of consistent measurements. In an earlier work [7] we have shown that this small discrepancy may be attributed, at least in part, to current data-reduction approaches, which neglect the effects of satellites and natural widths in extracting x-ray intensities from the spectra recorded by energy-dispersive Si(Li) x-ray detectors. We can thus conclude that f_{23} lies between 92 and 100 % of the IPM prediction. The situation for the L_1 subshell is much less clear. The theoretical values of f_{12} and f_{13} are not monotonic as a function of Z, because various Coster-Kronig transitions become energetically possible or impossible in particular atomic number ranges. Experimental values are few and their accuracy is difficult to discern.

A recent study [8] of L_1 deexcitation in xenon suggests that there is a large discrepancy between the IPM prediction and experiment for f_{12} and a smaller one for f_{13}. This suggested to us that we should expand our earlier work [9,10] on K and L x-ray emission from gadolinium in order to provide a further test in the atomic number region $50 < Z < 74$ where the $L_1L_2M_4$ and $L_1L_2M_5$ transitions are energetically forbidden.

II. OUTLINE OF THE METHOD

The method is similar to that of Marques, Martins, and Ferriera [11]. It involves measuring the L x-ray spectrum from a radionuclide undergoing decay by orbital electron capture. A simple decay scheme connecting the nuclear ground states of the parent and daughter nuclides is desirable so that the relative numbers of vacancies arising in the L_i subshells are accurately known. The spectrum is recorded in energy-dispersive fashion using a well-characterized Si(Li) detector, and the relative intensities of L_i x rays are obtained by a nonlinear least-squares fit to the spectrum.

The symbols e_K, e_{L_1}, etc. are used to denote the relative numbers of subshell vacancies produced directly by orbital electron capture. L subshell vacancies also arise indirectly from the deexcitation of the primary K shell vacancies

through both $K\alpha$ x-ray emission and *KLL* and *KLM* Auger-electron emission. The quantities n_{KLi} $(i=1,2,3)$ represent the probability of an L_i subshell vacancy resulting from an initial K vacancy. The fluorescence yields are ω_K, ω_1, ω_2, and ω_3. The L-subshell Coster-Kronig probabilities are f_{12}, f_{23}, and f_{13}; the overall probability that an L_1 vacancy shifts to the L_3 subshell is $f'_{13}=f_{12}f_{23}+f_{13}$. The symbols X_K, X_{L_1}, etc. denote the relative numbers of x rays emitted.

Determination of ω_1. We have

$$X_K=e_K\omega_K,$$

$$X_{L_1}=(e_{L_1}+e_K n_{KL_1})\omega_1.$$

Therefore

$$\omega_{L_1}=\frac{\omega_K}{A}\left(\frac{X_{L_1}}{X_K}\right), \quad \text{where} \quad A=\left(\frac{e_{L_1}}{e_L}\frac{e_L}{e_K}+n_{KL_1}\right). \tag{1}$$

Determination of ω_1 from Eq. (1) requires independent knowledge of ω_K.

Determination of f_{12}.

This is based upon the L_2 contribution to the x-ray spectrum,

$$X_{L_2}=(e_{L_2}+e_{L_1}f_{12}+e_K n_{KL_2}+e_K n_{KL_1}f_{12})\omega_2.$$

Therefore

$$f_{12}=\frac{\left(\frac{X_{L_2}}{X_K}\frac{\omega_K}{\omega_2}\right)-\frac{e_{L_2}}{e_L}\frac{e_L}{e_K}-n_{KL_2}}{A}. \tag{2}$$

Evaluation of f_{12} from this equation demands independent values for ω_2 and ω_K.

Determination of f_{13}.

The L_3 x-ray contribution is

$$X_{L_3}=[e_{L_2}f_{23}+e_{L_1}f_{13}+e_K n_{KL_3}+e_K n_{KL_2}f_{23}+e_K n_{KL_1}f'_{13}]\omega_3,$$

where $f'_{13}=f_{13}+f_{12}f_{23}$. Therefore

$$f'_{13}=\frac{\left(\frac{X_{L_3}}{X_K}\frac{\omega_K}{\omega_3}\right)-\frac{e_{L_2}f_{23}}{e_K}-n_{KL_3}-n_{KL_2}f_{23}}{A}. \tag{3}$$

Evaluation of f_{13} using Eq. (3) requires the existence of independent values for ω_K, ω_3, and f_{23}, together with the f_{12} value determined from Eq. (2).

Equations (1)–(3) define the necessary experiment as comprising measurements of the four x-ray intensity ratios X_L/X_K, X_{L_1}/X_L, X_{L_2}/X_L, and X_{L_3}/X_L, from which the necessary ratios on the left-hand side of each equation can be derived. We have reported earlier [9] an accurate measurement of X_L/X_K, and so the present work focusses upon the three L x-ray intensity ratios.

III. MEASUREMENT DETAILS

The radionuclide source consisted of approximately 5 MBq of ^{157}Tb deposited on a 50-μm-thick beryllium foil and covered with an aluminum film of thickness approximately 100 μg/cm^2. Details of the manufacture of the source and of its purity were given by us in Refs. [9] and [10].

The L x-ray spectrum was recorded using an Oxford Instruments lithium-drifted silicon detector [Si(Li)] that was 3 mm thick and 6 mm in diameter and that was equipped with a 0.025-mm-thick beryllium window. The resolution, as determined for manganese $K\alpha$ x rays (energy 5.9 keV) using a ^{55}Fe source, was 140 eV (full width at half-maximum). A tantalum collimator restricted x rays to a central circular region 2 mm in diameter. The aluminum-covered side of the source faced the detector. The counting rate during the ^{157}Tb experiments was 400 counts per second. In order to have excellent definition of even minor details of the spectrum, the total recorded intensity in the gadolinium L x-ray region was about 87 million counts.

Before measurements were taken, the resolution function (line shape) of this detector was determined in the 2–8 keV energy region by recording monoenergetic photon spectra provided by a double-crystal monochromator installed at the LURE storage ring at Orsay, France [12]. The same collimation conditions were used in that work.

IV. SPECTRUM FITTING

Because of the complexity of the L x-ray spectrum, in which there is significant overlap among the L_1, L_2, and L_3 series, the spectrum fitting is the most critical part of the experiment. This fitting was done with the nonlinear least-squares code GPPV, which is a general-purpose derivative of the Guelph PIXE software package GUPIX [13]. The main component of the spectrometer response was taken, as is customary, to be Gaussian. The parameters p_1 and p_2 in the linear relationship of Gaussian peak centroid to x-ray energy, i.e.,

$$c=p_1+p_2E, \tag{4}$$

were variables to be determined by the nonlinear least-squares procedure. Similarly, the parameters p_3 and p_4 in the relationship of the Gaussian peak width to energy, i.e.,

$$\sigma=(p_3+p_4E)^{0.5}, \tag{5}$$

were determined by the fit. Each peak in the spectrum is accompanied by a silicon $K\alpha$ x-ray escape peak displaced by the channel equivalent of 1.74 keV; the relative intensity of this escape peak was taken from the parametrization of Johansson [14].

Figure 1 displays the spectrometer response to monoenergetic x rays at 6 keV energy, together with the result of a least-squares fit of our model resolution function. The peak model comprises the Gaussian mentioned previously; an exponential low-energy tail; a long flat shelf extending to low energy; and an additional elevated shelf between the main line and the escape peak. The physical origins of these components are discussed by Papp *et al.* [15]. The parameters varied in this fit are listed in Table I.

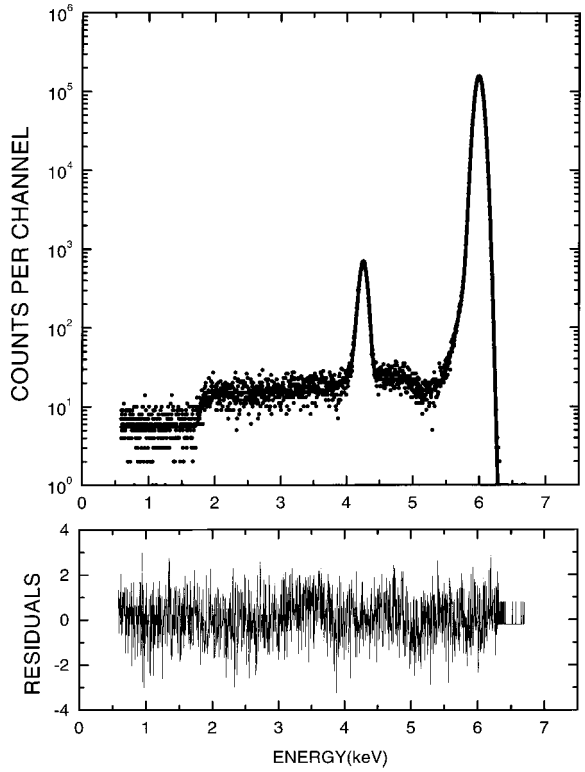

FIG. 1. Si(Li) spectra of 6 keV x rays: the upper panel shows the measured spectrum and the best fit (continuous curve); in the lower panel the residuals of the fit are displayed in units of one standard deviation.

From a set of such fits to monoenergetic photons in the 2–8-keV energy region, smooth functions were obtained for the energy-dependence of the coefficients of the tail and shelf functions.

Figure 2 displays the measured gadolinium L x-ray spectrum. Each peak in this spectrum is, in fact, the convolute of the Gaussian response function with the intrinsic Lorentzian distribution of x-ray energies. In fitting this spectrum, therefore, a Voigtian representation was used for each line, and the natural linewidths were taken from a recent compilation of measured and theoretical widths [16]. These widths, along with the line energies [17], are shown in Table II. The x-ray satellites were modeled in the same way as was described in Ref. [7]. Each of the 23 L x-ray peaks in the spectrum had associated with it one exponential tail and two shelves, as

TABLE I. Parameters varied in the least-squares fit of the 6-keV x-ray spectrum.

Feature	Parameters
Energy calibration	p_1, p_2
Width calibration	p_3, p_4
Gaussian	Height
Exponential tail	Relative height
	Relative slope
Long shelf	Relative height
Short shelf	Relative height
Background	Height
Escape Gaussian	Height

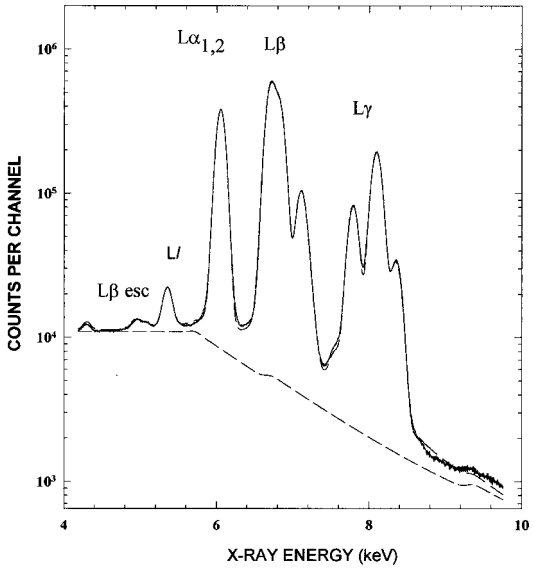

FIG. 2. Spectra of Gd L x rays: the continuous curve is the best fit to the data; the dashed curve is the background determined as described in the text.

prescribed by the resolution function measurements at LURE. A very small amount of additional high- and low-energy tailing was visible on the main $L\alpha$ and $L\beta$ lines, a finding that we attributed, on the basis of prior experience, to

TABLE II. Energies [17] and natural widths [14] of Gd L x-ray lines; the lines are divided here into seven groups; the height of the principal line (*) of each group was a variable of the fit. (In the energy column, bracketed values indicate values adopted to optimize the spectrum fit.)

Group	Line	Energy (keV)	Width (eV)
1	* L_3M_1	5.3621 (5.355)	14.6
2	* L_3M_5	6.0576 (6.054)	4.49
	L_3M_4	6.0256	4.87
	L_3M_2	5.5545	8.24
	L_3M_3	5.6988	11.04
	L_3N_1	6.8671	8.44
	L_3N_4	7.0933	4.70
	L_3N_5	7.1083	4.70
	L_3O_1	7.2067	3.70
	L_3O_4	7.2374	3.70
3	* L_2M_1	6.0495	11.90
4	*L_2M_4	6.7131 (6.716)	5.03
5	*L_2N_4	7.7808 (7.789)	4.90
	L_2N_1	7.5545	4.90
	L_2O_1	7.8942	3.70
	L_2O_4	7.9250	3.70
6	* L_1M_3	6.8316 (6.831)	11.90
	L_1M_2	6.6873	9.10
	L_1M_5	7.1904	5.70
	L_1M_4	7.1584	5.70
7	*L_1N_3	8.1047	9.60
	L_1N_2	8.0871 (8.075)	7.40
	$L_1N_{4,5}$	8.235	4.40
	$L_1O_{2,3}$	8.355 (8.352)	4.40

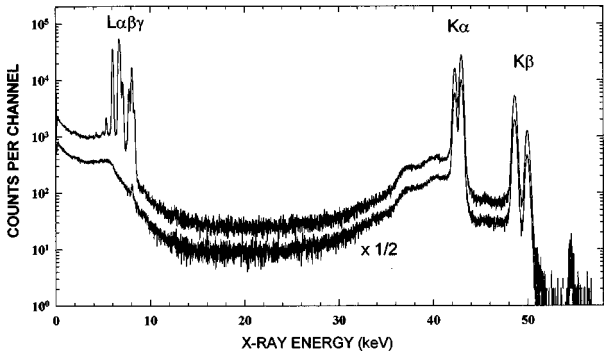

FIG. 3. Si(Li) spectra of Gd, spanning both the L and K x-ray regions. The lower spectrum was recorded with a 0.35-mm-thick aluminum absorber between source and detector.

noise effects; this noise contribution was described by two additional exponential tails (of very low intensity) common to all peaks in the spectrum. An additional short step was associated with the $L_1N_{2,3}$ lines, in order to represent the distortion from normal Lorentzian profile observed by Ohno and Lavilla [18]; this arises from many-body effects.

The continuum observed to the left of the L x-ray region is at least two orders of magnitude more intense than the expected flat shelves of the resolution function, and must, therefore, be associated with something other than the L x rays. The spectrum shown in Fig. 3 covers a much wider energy range set to include the K x-ray lines and the γ-ray peak in the 40–55-keV region. It is clear that degraded K x-ray events are responsible for the continuum that underlies the L x rays. To isolate this continuum, an 0.35-mm-thick aluminum absorber was interposed in front of the detector, thus effecting a strong reduction in the L x-ray intensity without significantly altering the continuum. This spectrum, which is shown in Fig. 4, is (apart from residual L x-ray contributions) the continuum component that must be included in the fit of the main L x-ray spectrum; it appears to

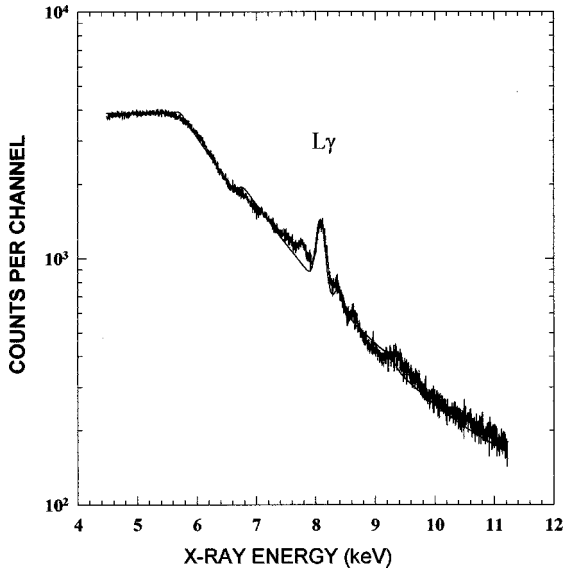

FIG. 4. Fit to the continuum component induced in the Si(Li) detector by the Gd K x rays and the 54.5-keV γ ray. The Gd L x-ray contribution has been minimized by use of a 0.35-mm-thick aluminum absorber.

have an approximately exponential dependence upon photon energy.

Inflections in the continuum are apparent at energies of approximately 5.7, 6.7, and 9.3 keV. These represent the Compton scattering at 180°, on the bound electrons of silicon, of $K\alpha$, $K\beta$, and 54.5-keV γ rays respectively. Felsteiner, Kahane, and Rosner [19] have, much earlier, demonstrated using a Si(Li) detector the downward energy shift of such Compton features relative to the values calculated for scattering on free electrons. In each case there is a distribution of approximately constant intensity going leftwards from the inflection (corresponding to the kinetic energies deposited by the scattered electron when the scattered photon angle ranges between 0° and 180°), and an exponential falloff going rightwards. To fit the spectrum of Fig. 4, we manipulated the capabilities of GPPV, using three peaks of very low intensity, each having an associated low-energy shelf and a high-energy exponential tail, each of much higher intensity than the peak itself. In addition, residual L x-ray lines were included as simple Gaussians. For this fit, the calibration parameters p_1-p_4 were fixed at values determined from the main spectrum fit. As shown in Fig. 4, the quality of fit is very good; the artifice of introducing the three weak lines does not cause serious distortion.

The continuum expression obtained in this manner was then employed as one component of the model used in the main L spectrum fit, with only one variable parameter, viz. the overall intensity of the continuum feature. This analysis of the continuum is clearly superior to the common approximation of assuming that the intensity varies linearly with photon energy across the L x-ray region.

We have shown elsewhere [10], using coincidence spectrometry, that the relative x-ray intensities within each of the L_1, L_2, and L_3 series agree very closely with Scofield's DF predictions [20]. In principle, therefore, we could (a) select only the three major lines (L_1M_3, L_2M_4, and L_3M_5) to be variables of the fit and (b) normalize all subsidiary lines within each series to bear the appropriate intensity ratio to the main line. This approach would be simpler than allowing all 23 lines to be variables. In practice, however, we chose an approach intermediate between these two extremes to determine the thickness of the aluminum absorber covering the source, and to effect the requisite corrections for x-ray attenuation. Seven line groups were defined, as summarized in Table II; within each group the line whose intensity was varied in the fit is marked by an asterisk. The main fit was repeated using various thicknesses for the aluminum absorbing film. For each assumed film thickness, the intensity ratios L_2M_4:L_2N_4 and $L_3M_{4,5}$:$L_3N_{4,5}$ were compared to the DF theoretical values [20]. The agreement was excellent at a thickness of 100 μg/cm^2, and this value was subsequently adopted.

Examination of the residuals between the measured and model spectra indicated that the fit could be improved by permitting small adjustments to the energies assumed for some of the L x-ray lines of gadolinium. The third column of Table II shows both the tabulated energies taken from the literature [17] and the adjusted energies that were employed in generating the final fit. Most of the adjustments are in the range 1–3 eV. The 7-eV change for the weak L_3M_1 line may partly occur because that line is very close in energy to the

TABLE III. Measured Gd L x-ray intensity ratios.

$$\frac{X_{L_1}}{X_L} = 0.437 \pm 0.018$$

$$\frac{X_{L_2}}{X_L} = 0.219 \pm 0.016$$

$$\frac{X_{L_3}}{X_L} = 0.344 \pm 0.003$$

escape peak of the much more intense $L_3N_{4,5}$ line. It is not a matter of concern in our case. However, it is our opinion that such deviation is also possible from the Bearden or Sevier energy values, because we have observed larger deviations between measured energies and the values given in the above tables. We will return to this question later. The L_2N_4 line energy to optimize the fit is 8 eV above the Sevier value; however, it is only 3 eV above the value recommended in the tables of Bearden [21]. The 12-eV shift necessary for the L_1N_2 line probably results from the non-Voigtian shape of that line, as discussed by Ohno and LaVilla [18] and Anagostopoulos, Borchert, and Lenz [22].

Concerning the energy values, our first question is whether the x-ray energy data obtained from electron impact ionization or photoionization measurements could be used in work on electron capture processes. There are two opinions in the literature. The first is that considerable differences (up to 10 eV or more) exist between the x-ray energies in electron capture processes and in ionization [23–25]. The other opinion is that the energy differences are in the range of 1 eV or a fraction of an electron volt [26,27]. Our second question concerns the accuracy of the available energy tables. Unfortunately, this is a significant question that we cannot address in a general sense here. However, good internal consistency could be expected within any particular overall data set. The internal consistency was checked and reported upon by Nigam and Agnihotri [28], who examined L_2Y-L_3Y x-ray energy differences for various shells denoted here by Y; they observed up to 5 eV variation in the L_2-L_3 differences derived from different x-ray energy pairs. The situation is presumably further complicated by chemical shifts of the x-ray energies. Overall then, the energy adjustments that we indicate in Table II are in the same range that has been discussed in the literature.

The reduced chi-square value of the final least-squares fit is 1.00 per million counts. An additional weak line had to be introduced at energy 7.2235 keV; this energy corresponds closely to the L_3O_3 line, whose intensity in the IPM is very low. It is possible that valence or solid state effects result in the intensity exceeding the predicted value. Such increase is not uncommon in x-ray spectra, examples being the $K\beta_5$ [29] and $K\beta_4$ [30,31] transitions. Table III presents our final x-ray intensity ratios; corrections for attenuation in the detector window, the intervening air, and the aluminum-cover foil have been made. Because of the very high overall intensity of the spectrum, the statistical errors in the final values for the intensity ratios X_{L_1}/X_L, X_{L_2}/X_L, and X_{L_3}/X_L are negligible. To generate an estimate of the uncertainty in these intensity ratios, the fit was repeated with the L_2N_4 energy fixed at the Sevier value. This fit was visibly very poor, and the reduced chi square increased to 133. Relative to the best fit, the changes in L_1, L_2, and L_3 x-ray intensities were, respectively, -0.7%, $+2.5\%$, and $+0.4\%$.

TABLE IV. Auxiliary quantities required for deriving L_1 subshell yields from the measured x-ray intensity ratios.

Quantity	Value	Source
ω_K	0.932 ± 0.004	[21]
n_{KL_1}	0.0328	See text
n_{KL_2}	0.2933 ± 0.004	See text
n_{KL_3}	0.5193 ± 0.0052	See text
e_{L_2}/e_{L_1}	0.0428	[9]
X_L/X_K	0.932 ± 0.030	[9]
e_L/e_K	3.88	[9]; see text
ω_2	0.177	IPM [2]
ω_3	0.169	IPM [2]
f_{23}	0.160	IPM [2]

V. ANALYSIS OF THE DATA

Evaluation of Eqs. (1)–(3) demands values for the various quantities other than the measured L x-ray intensity ratios. These values are summarized in Table IV.

The K-shell fluorescence yield ω_K is taken as 0.932 ± 0.004 from Bambynek's fit [32] to selected experimental data; this agrees with the IPM prediction (0.932) of Chen and Crasemann [33]. The quantities n_{KL_i} are described in detail by Bambynek *et al.* [34]; each of these contains a radiative contribution and a nonradiative contribution. Because the radiative width of the K shell is negligible, n_{KL_1} is determined essentially by Auger decay of the K vacancy. In the other two cases, the radiative component dominates. The radiative component involves ω_K, and the intensity ratios $X_{K\alpha_2}/X_{K\alpha_1}$ and $X_{K_\beta}/X_{K\alpha}$. We have used Scofield's DF predictions for these two ratios; these appear to be accurate at the 1% level in this region of the periodic table [35]. We have used the IPM K Auger rates of Perkins *et al.* [1] for the nonradiative components. The resulting values for the three quantities n_{KLi}, and their sum n_{KL}, together with uncertainties, are given in Table IV.

The value for e_{L_2}/e_{L_1} was derived from electron capture theory in Ref. [9], and from it we obtain the necessary ratios e_{L_1}/e_L and e_{L_2}/e_L. We take the quantity e_L/e_K from our own previous work [9], where it was derived from the measured ratio X_L/X_K using the equation

$$\frac{e_L}{e_K} = \left[\frac{X_L}{X_K} - \frac{n_{KL}\omega_{KL}}{\omega_K}\right]\frac{\omega_K}{\omega_{LL}}. \tag{6}$$

This involves the two mean L-shell fluorescence yields following K capture and L capture, ω_{KL} and ω_{LL}, respectively. These two mean yields have to be obtained by assuming a complete set of L subshell fluorescence and Coster-Kronig yields. In general, the mean L-shell fluorescence yield is given by

TABLE V. Present results and other recent measurements [8,36] of f_{12}, f_{13}, and ω_1 in the atomic number region $50 \leqslant Z \leqslant 70$.

	Z	Measured	IPM [2]
f_{12}	54	0.12 ±0.03 [8]	0.196
	62	0.19 ±0.03 [36]	0.212
	64	0.166±0.020	0.215
f_{13}	54	0.23 ±0.04 [8]	0.328
	62	0.18 ±0.03 [36]	0.332
	64	0.287±0.014	0.333
ω_1	62	0.067±0.010 [36]	0.075
	64	0.101±0.005	0.084

$$\overline{\omega} = N_1\nu_1 + N_2\nu_2 + N_3\nu_3, \tag{7}$$

where $N_1:N_2:N_3$ is the subshell vacancy distribution involved, and

$$\nu_1 = \omega_1 + f_{12}\omega_2 + (f_{12}f_{23} + f_{23})\omega_3,$$

$$\nu_2 = \omega_2 + f_{23}\omega_3,$$

$$\nu_3 = \omega_3. \tag{8}$$

In Ref. [9], adoption of the IPM predictions of Chen, Crasemann, and Mark [2] to derive ω_{KL} and ω_{LL} gave the value $R = 3.88$, with a 3% uncertainty at the 90% confidence level. In Ref. [9], we noted that currently available measurements of f_{13} and f_{23} in this region of atomic number tended to lie about 10% below the IPM predictions. We therefore derived an alternate value of R, based on ''experimental'' rather than IPM Coster-Kronig probabilities, by adjusting all three Chen, Craseman, and Mark Coster-Kronig values downwards by 10%. This adjustment gave $R = 4.12$. We then presented an average of these two R values as our final result. For the present purpose, we use the value 3.88.

The uncertainties in the three measured intensity ratios X_{L_i}/X_L have been propagated through Eqs. (1)–(3) to generate the corresponding uncertainties in ω_1, f_{12}, and f_{13}. In addition, the uncertainties in the various auxiliary quantities, as given in Table IV, have been propagated through the solution. The resulting uncertainties in each of the sought-after L_1 yields have then been added in quadrature to provide final estimates of experimental error. The results are collected and shown in Table V.

A new pair of values for ω_{KL} and ω_{LL} may now be derived from these results, and when these are substituted into Eq. (6) there is insignificant change in the derived e_L/e_K value. The results presented here are, therefore, entirely consistent with the work of Ref. [9].

VI. CONCLUSIONS

In common with other carefully conducted experiments in this region of the periodic table, our measurement indicates that the IPM theory overestimates the L_1 subshell Coster-Kronig yields quite considerably. Recent results in the atomic number region $50 < Z < 70$ are summarized in Table V. It is a straightforward matter to apply the current approach to several other simple decay schemes in order to generate improved L_1 subshell yields at other values of atomic number.

It follows from our results that the overall L_1 width is also overestimated by the IPM. Atomic level widths have recently been reviewed by Campbell and Papp [16]; while there are a large number of width measurements for the L_1 subshell and most of these fall below the IPM predictions, there is a dearth of data in the atomic number region $50 < Z < 70$. The Perkins *et al.* tabulation [1] indicates that 39% of the nonradiative L_1 width at $Z = 64$ is from Auger processes and 61% from Coster-Kronig processes. If we accept these IPM predictions for the Auger and for the radiative widths, then we can obtain a better estimate of the Coster-Kronig width from the equation

$$\frac{\Gamma_{CK}}{\Gamma_{CK} + \Gamma_R + \Gamma_A} = f_{12} + f_{13}. \tag{9}$$

This gives $\Gamma_{CK} = 1.68$ eV, and, in turn the overall width for the L_{13} level is 3.71 eV. This finding may be compared with the IPM prediction of 4.6 eV.

Finally, the current result provides the opportunity to refine the decay energy Q_{EC} relative to the value reported by Raman *et al.* [9]. The former value was the average of two numbers. The first of these was obtained by assuming the IPM yields for all three L subshells and the second was obtained via some estimates of the degree to which the latter might be in error. Using the L_1 yields determined herein together with the IPM yields for L_2 and L_3, the L/K electron capture ratio is 3.88 ± 0.15, and the decay energy is $Q_{EC} = 60.2 \pm 0.2$ keV. These two values may be compared with the corresponding results of $R = 4.0 \pm 0.2$ and $Q_{EC} = 60.0 \pm 0.3$ keV, as found in Ref. [9]. The conclusion of Ref. [9], viz. that L capture to the excited state at 54.5 keV is energetically impossible, remains unchanged.

ACKNOWLEDGMENTS

This work was financially supported by the Hungarian Research Fund under Contract Nos. T-026514 and T-016636, by the Natural Science and Engineering Research Council of Canada, and by the U.S. Department of Energy under Contract No. DE-AC05-96OR22464 with the Lockheed Martin Energy Research Corporation.

[1] S. T. Perkins, D. E. Cullen, M.-H. Chen, J. H. Hubbell, J. Rathkopf, and J. H. Scofield, Lawrence Livermore Laboratory Report No. UCRL-50400, 1991, Vol. 30.

[2] M.-H. Chen, B. Crasemann, and H. Mark, Phys. Rev. A **24**, 177 (1981).

[3] I. Orlic, C. H. Sow, and S. M. Tang, At. Data Nucl. Data Tables **56**, 159 (1994).

[4] *Handbook of X-Ray Spectrometry*, edited by R. E. Van Grieken and A. A. Markowicz (Marcel Dekker, New York, 1993).

[5] M. O. Krause, J. Phys. Chem. Ref. Data **8**, 307 (1979).
[6] W. Jitschin, in *X-Ray and Inner-Shell Processes*, Knoxville, 1990, edited by T. A. Carlson, M. O. Krause, and S. T. Manson (AIP, New York, 1990); in *Proceedings of the Fifteenth Conference on X-Ray and Inner-Shell Ionization (X90)*, edited by Invited Presentations, AIP Conf. Proc. No. 215 (AIP, New York, 1990), p. 408.
[7] T. Papp, J. L. Campbell, and S. Raman, Phys. Rev. A **49**, 729 (1994).
[8] W. Jitschin, R. Stotzel, T. Papp, M. Sarkar, and G. D. Doolen, Phys. Rev. A **52**, 977 (1995).
[9] S. Raman, J. L. Campbell, A. Prindle, R. Gunnink, and J. C. Palathingal, Phys. Rev. C **46**, 2241 (1992).
[10] T. Papp, J. L. Campbell, and S. Raman, J. Phys. B **26**, 4007 (1993).
[11] M. I. Marques, M. C. Martins, and J. G. Ferriera, Phys. Scr. **32**, 107 (1985).
[12] J. L. Campbell, G. Cauchon, M.-C. Lepy, L. McDonald, J. Plagnard, P. Stemmler, W. J. Teesdale, and G. White, Nucl. Instrum. Methods Phys. Res. A (to be published).
[13] J. A. Maxwell, W. J. Teesdale, and J. L. Campbell, Nucl. Instrum. Methods Phys. Res. B **95**, 407 (1995).
[14] G. I. Johansson, X-Ray Spectrom. **11**, 194 (1982).
[15] T. Papp, J. L. Campbell, D. Varga, and G. Kalinka, Nucl. Instrum. Methods Phys. Res. A **412**, 109 (1998).
[16] J. L. Campbell and T. Papp, X-Ray Spectrom. **24**, 307 (1995).
[17] K. D. Sevier, At. Data Nucl. Data Tables **24**, 352 (1979).
[18] M. Ohno and R. E. La Villa, Phys. Rev. B **39**, 8852 (1989).
[19] J. Felsteiner, S. Kahane, and B. Rosner, Nucl. Instrum. Methods **118**, 253 (1973).
[20] J. H. Scofield, Phys. Rev. A **10**, 1507 (1974).
[21] J. A. Bearden, Rev. Mod. Phys. **39**, 78 (1967).
[22] D. F. Anagostopoulos, G. L. Borchert, and St. Lenz, Phys. Lett. A **194**, 93 (1994).
[23] P. T. Springer, C. L. Bennett, and P. A. Baisden, Phys. Rev. A **31**, 1965 (1985).
[24] K. Riisager and A. Rosen, Phys. Rev. A **34**, 3454 (1986).
[25] P. T. Springer, C. L. Bennett, and P. A. Baisden, Phys. Rev. A **35**, 679 (1987).
[26] G. L. Borchert, T. Rose, P. G. Hansen, B. Jonson, and H. L. Ravn, Z. Naturforsch. Teil A **42**, 781 (1987).
[27] P. G. Hansen, B. Jonson, G. L. Borchert, and O. W. B. Schult, in *Atomic Inner Shell Physics*, edited by B. Crasemann (Plenum, New York, 1985), p. 237.
[28] A. N. Nigam and A. K. Agnihotri, Physica C **133C**, 225 (1987).
[29] I. Torok, T. Papp, J. Palinkas, M. Budnar, A. Mulheisen, J. Kawai, and J. L. Campbell, Nucl. Instrum. Methods Phys. Res. B **114**, 9 (1996).
[30] T. Ludziejewski, P. Rymuza, Z. Sujkwoski, B. Boschung, J.-Cl. Dousse, B. Galley, Z. Halabuka, Ch. Heren, J. Hoszowska, J. Kern, Ch. Rheme, and M. Polaski, Phys. Rev. A **52**, 2791 (1995).
[31] J. Hoszowska and J.-Cl. Dousse, J. Phys. B **29**, 1641 (1996).
[32] W. Bambynek, in *Proceedings of the International Conference on X-ray and Inner-Shell Processes in Atoms, Molecules and Solids*, edited by A. Meisel (VEB Druckerei, Thomas Munzer, Langensalza, 1984).
[33] M.-H. Chen, B. Crasemann, and H. Mark, Phys. Rev. A **25**, 391 (1982).
[34] W. Bambynek, B. Crasemann, R. W. Fink, H.-U. Freund, H. Mark, C. D. Swift, R. E. Price, and P. V. Rao, Rev. Mod. Phys. **44**, 716 (1972).
[35] J. L. Campbell, P. L. McGhee, J. A. Maxwell, R. W. Ollerhead, and B. Whittaker, Phys. Rev. A **33**, 986 (1986).
[36] R. Stotzel, U. Werner, M. Sarkar, and W. Jitschin, J. Phys. B **25**, 2295 (1992).